Lagrangian-Eulerian Micromotion and Wave Heating in Nonlinear Self-Excited Dust-Acoustic Waves

Chen-Ting Liao, Lee-Wen Teng, Chen-Yu Tsai, Chong-Wai Io, and Lin I

Department of Physics and Center for Complex Systems, National Central University, Jhongli, Taiwan 32001, Republic of China

(Received 4 September 2007; published 6 May 2008)

We investigate particle-wave microdynamics in the large amplitude self-excited dust acoustic wave at the discrete level through direct visualization. The wave field induces dust oscillations which in turn sustain wave propagation. In the regular wave with increasing wave amplitude, dust-wave interaction with uncertain temporary crest trapping and dust-dust interaction lead to the transition from cyclic to disordered dust motion associated with the liquid to the gas transition, and anisotropic non-Gaussian heating. In the irregular wave, particle trough-trapping is also observed, and the heating is nearly Gaussian and less anisotropic.

DOI: 10.1103/PhysRevLett.100.185004 PACS numbers: 52.27.Lw, 05.45.−a, 52.25.Gj, 52.35.Fp

Microscopically, the background medium supporting acoustic type density waves, e.g., the ion acoustic wave in plasma [1] or the sound wave in gas, is a many body system. Particles not only interact with but also constitute the wave. In addition to the macroscopic mean field, the spatio-temporal heterogeneity at the discrete level makes the particle motion a complicated problem beyond the intuitive expectation of sinusoidal oscillation. Moreover, the possible non-Gaussian heating through the above non-Markovian particle-wave interaction, and how the induced individual motion in turn self-sustains the structure and propagation of the macroscopically coherent wave, especially for the large amplitude nonlinear wave, are also poorly explored nonlinear complex problems. In the kinetic model for the electro-static wave in collisionless plasmas [1], the particle interaction with washboard-type wave mean field leads to interesting particle trapping, heating, and wave damping. Nevertheless, the existing perturbation approaches treating the system as a continuous medium without direct microscopic measurement are still insufficient to understand the above microscopic issues.

The dusty plasma consists of dust particles negatively charged ($\sim 10^4$ electron/dust) and suspended in a low-pressure gaseous plasma background. The dust acoustic wave (DAW) associated with longitudinal dust particle oscillation has been predicted theoretically [2,3] and observed experimentally in various dusty plasmas [4–12]. It belongs to the family of acoustic type density wave. Particles interact with each other through the screened Coulomb field. Large amplitude DAWs can be self-excited under the free energy sources such as ambipolar diffusion field and ion streaming even in a collisional background, and other feedback mechanisms such as the unfrozen charges on the dust particles and the unfrozen ionization of the background plasma [2,6–9,13,14]. Macroscopic fluid models and measurements were mainly used in the previous studies [2–9,13,14]. Only few experiments used particle imaging techniques, e.g., studying the spatial distribution of particle velocity for DAW spatial growth [10], observing the wave-resonant particle, and measuring the velocity of and force on the particle in a DAW [11].

In this Letter, using a self-excited regular DAW and an irregular DAW with small to large wave amplitudes and different degrees of wave ordering as examples, we experimentally address wave-particle interaction, particle trapping, induced nonlinear particle motion and heating, and how the nonlinear motion sustains the wave propagation. The information from the spatio-temporal evolutions of the dust trajectory, velocity, and density using high-speed (300 Hz) digital microscopy enables the Lagrangian in addition to the Eulerian description for particle-wave microdynamics, which helps to understand the generic micro-behaviors of acoustic type density waves.

The experiment is conducted in a cylindrical symmetric rf dusty plasma system as described elsewhere [15]. A hollow coaxial cylindrical trap with 3-cm inner diameter and 14-mm height is put on the bottom electrode to confine the dusty plasma with polystyrene particles (5 μm diameter). The weakly ionized glow discharge ($n_e \sim 10^9$ cm^{-3}) is generated in Ar gas at 170 mTorr using a 14-MHz rf power system at a few watt power. The dust mass and the dust charge are 6.9×10^{-11} g/dust and about 5000 e/dust, respectively. The Debye length λ_D is about 100 μm. The suspended dust particles are aligned by the downward vertical ion flow to form vertical chains [15,16]. The interchain distance is 0.3 mm. The system can be tuned from the quiescent quasi-2D liquid state organized by the vertical chains to the self-excited wave state by increasing rf power. An expanded thin vertical Nd-YAG laser sheet through the center vertical axis is used for particle illumination. Dust particle motions are monitored through digital video microscopy at 300 Hz frame rate.

Figures 1(a)–1(c) show the snap shots of the quiescent particle positions and the sequential temporal evolution before and after the onset of the downward traveling

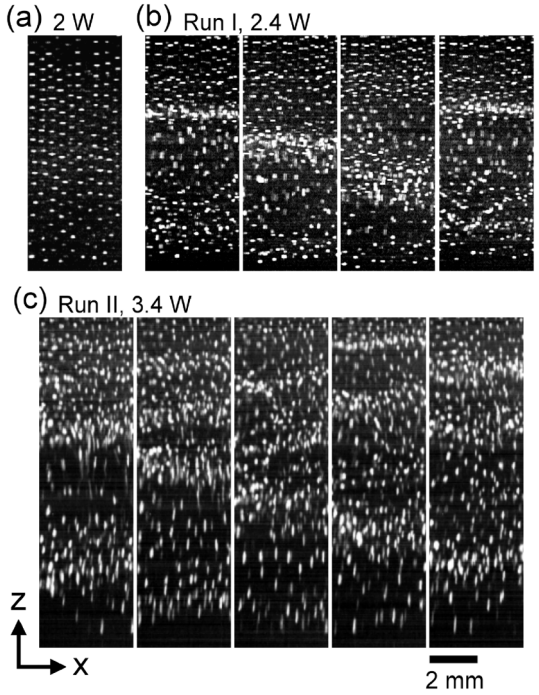

FIG. 1. The side view of the suspended dust particles. (a) At 2.0 W rf power, before the onset of DAW. Particles are in the liquid state with vertical chain structure aligned by the downward ion wind. (b) and (c) The sequential snap shots with 1/60 s time interval showing the downward propagating DAW at 2.4 W (run I) and 3.4 W (run II) rf power for the regular and irregular wave states, respectively.

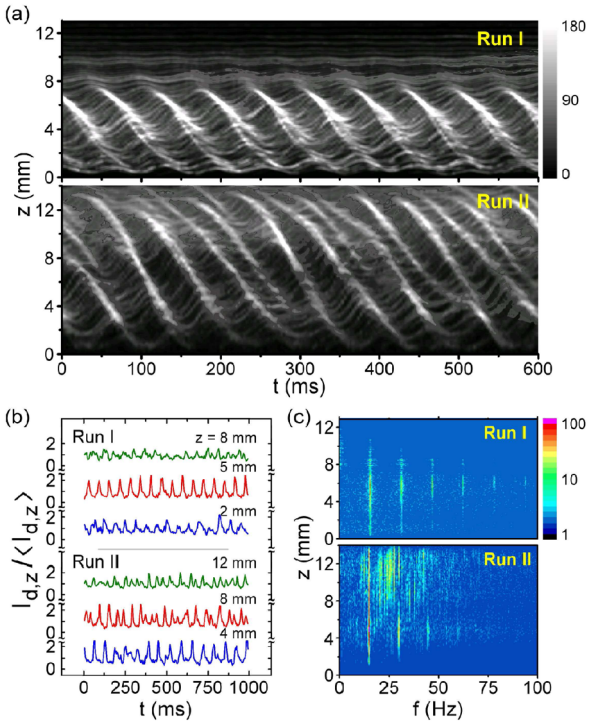

FIG. 2 (color online). (a) The plots of the image intensity I_d in z-t plane showing the regular periodic wave pattern (run I) and the irregular pattern (run II) with phase defects. (b) The temporal evolution of $I_{d,z}/\langle I_{d,z}\rangle$ measured at different z for the two runs. (c) The contour plots of power spectra in the z-f space for the two runs. The power spectra for run I shows fundamental frequency at 16 Hz and clear peaks of higher harmonics, especially in the center region with high amplitude I_d oscillation. The spectra for run II are more spread especially in the upper region.

DAW at 170 mTorr background pressure and 2.0 W, 2.4 W (run I) and 3.4 W (run II) rf power, respectively. Figure 2(a) shows the spatio-temporal evolution of the coarse-grained intensity I_d (averaged over 3 mm horizontally and 0.3 mm vertically along the center vertical axis of each image) in the z-t plane (z is the vertical position). The intensity is approximately proportional to the dust particle density n_d. The bright region corresponds to the wave crest. Figure 2(b) also depicts the temporal evolution of $I_{d,z}$ normalized by the time averaged intensity $\langle I_{d,z}\rangle$ at different z. Under the free energy from the downward ion wind, DAW is initiated from the upper part ($z > 11$ mm) with small amplitude oscillation. The instability quickly grows with decreasing z. For run I, the waveform becomes pulse-like starting from $z = 7$ mm (e.g., see the spiking oscillation at $z = 5$ mm). It manifests the nonlinear nature of the wave. The amplitude then gradually decreases while approaching the bottom sheath boundary ($z = 1$ mm). The fundamental frequency at 16 Hz and its harmonics can be observed in the power spectra [Fig. 2(c)]. The wavelength and the phase velocity are about 4.5 mm and 70 mm/s, respectively.

Particles mainly exhibit vertical oscillation in the DAW. Figure 3(a) shows particle motion in the z-t space and $z - v_z$ phase space, where v_z is the vertical velocity. At the first glance, the oscillating phases for different trajectories are quite disordered. However, using the wave crest (bright region) in the $I_d(z, t)$ plot as a background reference, common rules of their behaviors and interaction with the wave can be easily found. Dust particles are negatively charged. A test particle sees a potential energy U roughly oscillating in phase with n_d oscillation. In the wave frame z', the particle with total energy E slows down while entering the crest region [see the sketch in 3(b)]. In the laboratory frame, the upward moving particle is decelerated by the downward traveling crest front. It moves downward with the crest at a slightly slower speed than the crest, and then goes up (accelerated upward by the crest rear) again to repeat the oscillation [see the sketch in Fig. 3(c)]. For run I, the small but growing amplitude of the wave with the decreasing z in the upper region ($z > 7$ mm) only causes cyclic motion with growing excursion range in the phase space [e.g., particles A, B, and C in Fig. 3(a)]. It keeps the particles in the liquid state with long time correlation between the positions of the neighboring particles.

However, in the middle region with large amplitude DAW (7 mm $> z > 3$ mm), some wave-resonant particles can travel over uncertain long distance with crests (i.e., trapping in the *ghost region*, using a nonlinear dynamics jargon), in which the particle velocity relative to the crest is reduced to nearly zero. As illustrated by Figs. 3(b) and

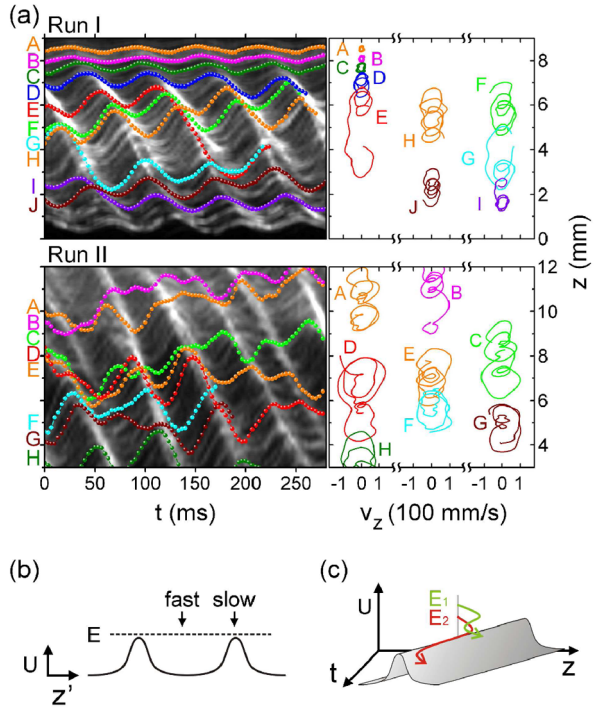

FIG. 3 (color online). (a) The temporal evolution of particle vertical displacements (left) using the contour plot of $I_d(z, t)$ as a reference and the corresponding trajectories in the z-v_z phase space (right) for the two tested runs. (b) The sketch showing the slow motion of a dust particle with total energy E around the crest region of a washboard-type field in the wave frame z'. (c) The sketch showing how the trajectories of two particles at different total energies E_1 and E_2 oscillate with different trapping times when they encounter a traveling wave crest in the laboratory frame.

3(c), the above traveling distance (or the trapping time) is quite sensitive to the state entering the crest. The real potential field is not so smooth as that in the above cartoons at the discrete level. The trapping time can be easily further affected by local dust-dust interaction even under the slight variation of the local dust configuration. This leads to the observed disordered excursion in the phase space [particles D to J for run I in Fig. 3(a)], and turns dust particles into the gas state after losing spatio-temporal correlation. For example, particles F to H have similar initial condition at $t = 0$ s, but their trajectories quickly diverge. Particle G is nearly trapped in the crest region and shows long distance downward excursion up to $t = 70$ ms, but with short distance downward excursion in the next cycle. Particles F and H more quickly escape from the crest and show smaller amplitude oscillation. Similar behavior is also demonstrated by particles E and F at $t = 125$ ms. The wiggling of the trajectories in the z-v_z space evidences the dust-dust interactions by the local heterogeneity. In the lower region with smaller amplitude n_d fluctuation, the motion becomes less disordered.

We further measure the Lyapunov exponent λ from the exponent of the averaged temporal divergent rate of the distance $\delta X(t + \Delta t)$ between the states of two particles in the v_z-z phase space with small initial distance $\delta X(t)$ [i.e., $\langle \delta X(t + \Delta t)/\delta X(t) \rangle = \exp(\lambda \Delta t)$] [17]. In each region, 500 trajectory pairs are used for the statistical measure. λ changes from -0.01 to 0.97, and 0.65 s^{-1} from the upper to the center and the lower regions, respectively. It again manifests the transition from the liquid state with cyclic motion to the gas state with disordered motion and exponentially diverging trajectories.

Dust particles also constitute the washboard-type wave field. In the wave frame, the low dust velocity in the crest region self-consistently maintains the high density of the crest under the mass conservation. In the laboratory frame, the piling up (compression) of the decelerated particles in the crest front and the depletion of the upward escaping particles in the crest rear self-consistently sustain the downward advance of the crest.

Regardless of the above disordered particle oscillation, the $I_d(z, t)$ pattern looks quite regular for run I [Figs. 2(a) and 2(b)]. Particle trough-trapping has not been found. For run II at higher rf power (3.4 W), the irregular waveform starts in the upper region (Fig. 2). It exhibits phase defects with wave-crest merging and annihilation. The irregular n_d fluctuation with faster n_d amplitude variation and larger crest speed variation (45 to 140 mm/s), especially for the upper part, is associated with the more disordered particle motion. In addition to the similar trapping in the crest, some particles do not even have sufficient velocity to reach the high amplitude crest. Trough trapping is evidenced by their downward motion before hitting the crest [e.g., particle G and particle C at 75 ms for run II in Fig. 3(a)]. After a while, they are pushed upward again by other upward moving particles (e.g., particles E and H), and climb over the nearby crest.

The wave heats up dust particles. Figure 4(a) depicts the double-hump non-Gaussian v_z histograms for run I, measured from the displacements with 3.33 ms time interval in a few typical bands centered at different height z and each with 2 mm in vertical width. The root mean square velocity σ_z gradually increases with the increasing crest amplitude and reaches the maximum in the middle region [run I in Fig. 4]. Note that the histogram for a purely sinusoidal velocity oscillation has two symmetric sharp peaks at both edges (not shown). The speeds at the peaks of our humps are lower than the wave speed (e.g., about 39 and 70 mm/s, respectively at $z = 5$ mm). It again supports that the speeds of most particles temporarily trapped in the crest region are lower than the wave speed. The broadened tail is contributed by the small fraction of resonant particles moving at nearly the same velocity with the crest and the additional local dust-dust collisions. The slightly skewed histograms in the middle and the lower regions for run I reflect the slight asymmetry between the upward and the downward motion, broken by the downward propagating nonlinear wave. The particle usually gradually escalates after a few oscillating cycles and then travels long distant downward [Fig. 3(a)]. The self-excited wave heats

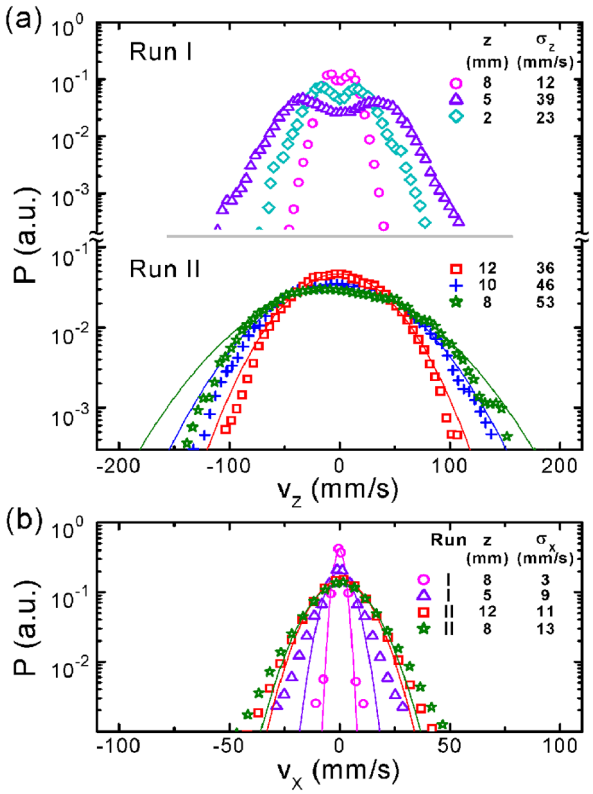

FIG. 4 (color online). (a) and (b) The histograms for the longitudinal and transverse velocity histograms at different z for the two runs, respectively. σ corresponds to the root mean square velocity. The thin curves indicate the best Gaussian fit.

up particles to average energy about 33, 290, and 106 eV at $z = 8$, 5, and 2 mm, respectively.

For the irregular run II [Fig. 3(b)], the faster memory washout associated with the more disordered particle motion smooths up the two bumps in the v_z histograms. Below $z = 8$ mm, n_d has large oscillation amplitude associated with the higher wave crest velocity (ranged from 80 to 120 mm/s). It widens σ_z to 53 mm/s at $z = 8$ mm. The v_z histogram exhibits faster dropping tails than the Gaussian distribution (the histograms for $z < 8$ mm region are about the same as that at $z = 8$ mm, but not shown). It is still slightly skewed. The symmetric and nearly Gaussian v_z histograms in the upper region ($z > 9$ mm) manifests the memory washing process through the more irregular wave interaction under a broader distribution of crest amplitudes and velocities (45 to 90 mm/s) [see the more disordered $I_d(z, t)$ evolutions and the corresponding wide band spectra in Fig. 2(a) and 2(b)]. The lower averaged crest velocity also leads to the smaller σ_z (36 mm/s at $z = 12$ mm).

The wave heating is anisotropic. Figure 4(b) shows the histograms of v_x with slower descending non-Gaussian tails for the two runs. $\sigma_x/\sigma_z = 0.24$ and 0.23, for run I at $z = 8$ and 5 mm, respectively, and it increases to 0.31 and 0.33 for run II at $z = 12$ and 8 mm, respectively. It implies the vertical electric field dominated heating in the downward propagating DAW. The increased heterogeneity in run II enhances the transverse energy transfer and makes the heating less anisotropic.

In conclusion, we experimentally construct a Lagrangian-Eulerian picture for the nonlinear particle-wave microdynamics. We found the following: (a) The upward moving dust is pushed downward and then upward by the traveling (downward) wave front and wave rear, respectively. It causes dust longitudinal oscillation. (b) The piling up and depleting of dusts in the front and the rear of the crest, respectively, sustain the downward propagation of the crest. (c) The increasing wave amplitude enhances dust crest trapping. The uncertain trapping time and the dust-dust interaction induce the transition from the liquid state with ordered cyclic particle motion to the gas state with the disordered oscillation even in the regular wave. (d) In the irregular wave with fluctuating crest speed and amplitude, dust motion becomes more disordered. Temporary trough trapping is also observed. (e) The DAW heats up dusts anisotropically with $0.23 < \sigma_x/\sigma_z < 0.33$. It induces non-Gaussian v_z and v_x histograms with high v_z tails from wave-resonant particles. The variance increases with wave crest speed and amplitude. The distribution becomes more Gaussian-like for the irregular wave.

This work is supported by the National Science Council of the Republic of China under Contract No. NSC95-2112-M008-015.

[1] e.g. F. F. Chen, *Introduction to Plasma Physics* (Plenum Press, New York, 1974), Chap. 7, p. 199.
[2] N. N. Rao, P. K. Shukla, and M. Y. Yu, Planet. Space Sci. **38**, 543 (1990).
[3] P. K. Shukla, Phys. Scr. **45**, 504 (1992).
[4] J. H. Chu, Ji-Bin Du, and L. I, J. Phys. D **27**, 296 (1994).
[5] A. Barkan, R. L. Merlino, and N. D'Angelo, Phys. Plasmas **2**, 3563 (1995).
[6] A. V. Zobnin *et al.*, JETP **95**, 429 (2002).
[7] V. E. Fortov *et al.*, Phys. Plasmas **10**, 1199 (2003).
[8] A. Piel, *et al.*, Phys. Rev. Lett. **97**, 205009 (2006).
[9] T. Trottenberg, D. Block, and A. Piel, Phys. Plasmas **13**, 042105 (2006).
[10] E. Thomas, Jr., Phys. Plasmas **13**, 042107 (2006).
[11] M. Schwabe *et al.*, Phys. Rev. Lett. **99**, 095002 (2007).
[12] C. T. Liao *et al.*, in *Proceedings of the 16th IEEE International Pulsed Power Conference* (IEEE, New York, 2007), p. 1110.
[13] P. Kaw and R. Singh, Phys. Rev. Lett. **79**, 423 (1997).
[14] A. A. Mamun and P. K. Shukla, Phys. Plasmas **7**, 4412 (2000).
[15] H. Y. Chu *et al.*, Phys. Rev. Lett. **90**, 075004 (2003).
[16] e.g. M. Nambu, S. V. Valdimirov, and P. K. Shukla, Phys. Lett. A **203**, 40 (1995).
[17] S. H. Strogatz, *Nonlinear Dynamics and Chaos* (Addison-Wesley, Reading, 1994), Chap. 9.